Iwao Nitta, Tero Hottinen, Olli Himanen and Mikko Mikkola, Inhomogeneous compression of PEMFC gas diffusion layer – Part I. Experimental, Journal of Power Sources, accepted for publication, Dec 2006.

Available online at www.sciencedirect.com
ScienceDirect
Journal of Power Sources xxx (2006) xxx–xxx
JOURNAL OF POWER SOURCES
www.elsevier.com/locate/jpowsour

Inhomogeneous compression of PEMFC gas diffusion layer Part I. Experimental

Iwao Nitta [a,*], Tero Hottinen [b], Olli Himanen [a], Mikko Mikkola [a]

[a] *Helsinki University of Technology, Laboratory of Advanced Energy Systems, P.O. Box 2200, 02015 HUT, Finland*
[b] *Wärtsilä Corporation, Tekniikantie 14, 02150 Espoo, Finland*

Received 4 September 2006; received in revised form 10 November 2006; accepted 14 November 2006

Abstract

This paper presents a study on the effect of inhomogeneous compression of gas diffusion layer (GDL) caused by the channel/rib structure of flow-field plate. The experimentally evaluated properties are GDL intrusion into the channel, gas permeability, in-plane and through-plane bulk electric conductivities, and contact resistances at interfaces as a function of compressed thickness of GDL. It was found that the GDL is compressed very little under the channel whereas GDL under the rib is compressed to gasket thickness. The compression of GDL reduces gas permeability and contact resistance, and improves bulk conductivity. Hence, the inhomogeneous compression of GDL may lead into significant local variation of mass and charge transport properties in the GDL. These effects have been ignored in most of the published modeling studies. This contribution, part I, covers the experimental setup and measurement results, and a model which takes the inhomogeneous compression of GDL into account is presented in part II.

Keywords: PEMFC; Gas diffusion layer; Inhomogeneous compression; Contact resistance; Gas permeability; Electrical conductivity

1. Introduction

Proton exchange membrane (PEM) fuel cells are electro-chemical devices that convert the chemical energy of reactants directly into electrical energy. This technology enables high efficiency and energy density compared to conventional internal combustion engines, thereby making the technology attractive for automotive, portable, and stationary applications. Furthermore, the only exhaust from PEM fuel cells is water, which makes them favorable from the environmental point of view.

PEM fuel cell consists of bipolar plates with channels machined on either side for reactant distribution over the electrode surface, membrane electrode assembly (MEA) where the electro-chemical reactions and proton transport takes place, and porous gas diffusion layers (GDL) sandwiching the MEA. Among the components of PEM fuel cell, much research effort has been put on catalysts, membranes and bipolar plates.

Until recently, less attention has been paid to GDL even though it plays an important role in fuel cell operation. The main functions of GDL are to provide a passage for reactant access and product water removal, to conduct electricity and heat between adjacent components, and to provide mechanical support for the MEA. These functions impose requirements on the electrical and mechanical properties of GDLs, i.e. high gas permeability and suitable water management properties, electrical and thermal conductivity, and chemical and physical durability. Typically, GDLs are made of highly porous carbon-fiber based paper or cloth.

The properties of GDL and interfaces between the GDL and the electrode and flow field plate are strongly dependent on compression pressure. Generally speaking, increasing compression improves electrical and thermal conductivity, and impedes reactant transport and water removal. A flowchart of the effects of increasing compression is presented in Fig. 1.

Pressure onto the GDL is exerted by the flow field plates, which usually feature flow channels for reactant distribution. The rib/channel-structure creates an inhomogeneous compression distribution, because the GDL under ribs is compressed to gasket thickness while GDL under the channels remains mostly uncompressed and intrudes into the channel, see Fig. 2.

DOI of original article:10.1016/j.jpowsour.2006.10.076.
* Corresponding author. Tel.: +358 9 451 3158; fax: +358 9 451 3195.
E-mail address: iwao.nitta@hut.fi (I. Nitta).

0378-7753/$ – see front matter © 2006 Elsevier B.V. All rights reserved.
doi:10.1016/j.jpowsour.2006.11.018

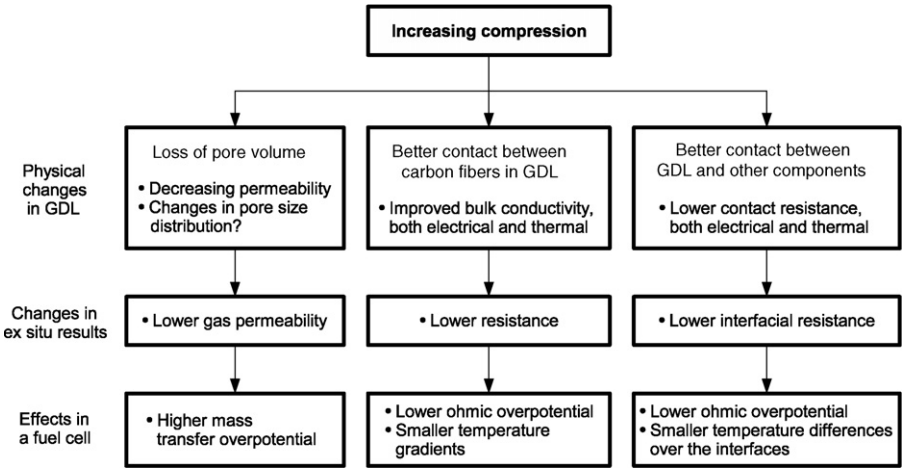

Fig. 1. The effects of increasing compression of GDL.

Inhomogeneous compression distribution leads into spatial variation of GDL and interface properties. Fluid permeability is lower in the GDL under the ribs due to loss of porosity, which increases mass transport overpotential in those areas compared to areas under the channel. Similarly, electrical and thermal bulk conductivities are improved and contact resistances at the interfaces between the GDL and electrode and flow field plate are smaller than those under the channel.

These effects exist in all fuel cells with normal flow field plates but cannot be measured directly due to small scale of the phenomena. Thus, the only available option is to characterize the GDLs *ex situ* and model the effect. Furthermore, most of the published fuel cell models do not account for the inhomogeneous compression of the GDL and its effects. Usually GDL thickness, porosity, contact resistances and conductivities are assumed constant over the cell area. There may be a significant discrepancy between the modeled results and practical situation due to these assumptions. Only few studies, such as by Sun et al. [1] and Zhou et al. [2], were found by authors, in which the effect of inhomogeneous compression of GDL is taken into account. However, Sun et al. did not account for the contact resistance, and Zhou et al. ignored the effect of compression on the bulk conductivity of GDL.

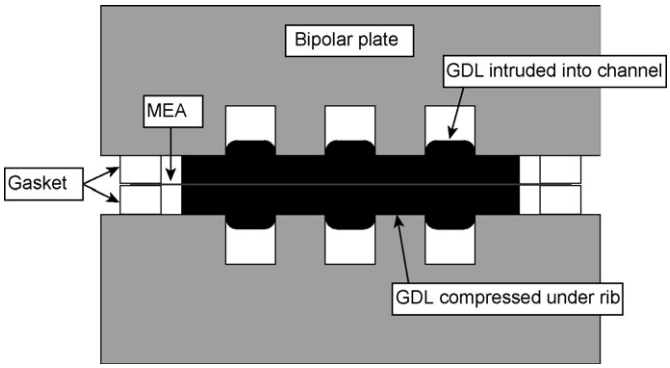

Fig. 2. Schematic illustration of GDL deformation under compression. The GDL partially intrudes into the channels and the parts under the ribs are more compressed.

Effects of compression and GDL properties on fuel cell performance have been studied by several groups, e.g. Lee et al. [3], Ge et al. [4], and Ihonen et al. [5]. The results show that the compression force and physical properties of GDL must be considered together and there is an optimum compression pressure and compressed thickness for each GDL which trades off the competing demands of mass, charge and heat transport within the GDL.

GDL parameters, such as permeability, both electric and thermal conductivity and contact resistance between components have been investigated, e.g. Dohle et al. [6], Williams et al. [7], Feser et al. [8], Ihonen et al. [9], Mishra et al. [10], Wang and Turner [11], Vie and Kjelstrup [12] and Khandelwal and Mench [13]. However, in contact resistance studies [9–11], the effect of compression on bulk conductivity was ignored. Furthermore, Ihonen et al. [9] and Natarajan and Nguyen [14] found that fuel cell operating parameters or experimental operating conditions also affected the contact resistance. Relating to compression, it has been observed that excessive compression damages the carbon fibers in GDL materials, e.g. Wilde et al. [15], Escribano et al. [16] and Matsuura et al. [17].

Some of the actual GDL properties have been included in published fuel cell models. Chu et al. [18] considered the non-uniform porosity due to presence of water in GDL. Berning and Djilali [19], Natarajan and Nguyen [20], Inoue et al. [21], and Jang et al. [22] modeled the mass and charge transport with various operating parameters and studied the impact of geometric parameters of flow field and material properties of GDL such as porosity and thickness. Pharoah [23] applied anisotropic gas permeability into their models, and Meng and Wang [24] and Pharoah et al. [25] modeled the effect of anisotropic electrical conductivity and observed large variations between isotropic and anisotropic cases. However, the authors did not find any models that took into account the spatial variations in permeability, and electrical and thermal conductivity due to inhomogeneous compression. This may cause significant errors in modeled results, e.g. in the prediction of current density distribution, and therefore it is worth studying how the compression pressure affects charge and species transport.

Please cite this article in press as: I. Nitta et al., J. Power Sources (2006), doi:10.1016/j.jpowsour.2006.11.018

The purpose of this contribution is to experimentally evaluate the GDL parameters (GDL intrusion into channel, gas permeability, electrical bulk conductivities and contact resistances) as a function of compressed thickness. Determination of thermal conductivity and thermal contact resistance was left outside this work. The evaluated values will be used in a modeling study, in which the effects of inhomogeneous compression on the local phenomena are taken into account. These results of modeling studies are given in part II of this contribution [26].

2. Experimental

A commercial gas diffusion media, SGL SIGRACET 10-BA carbon paper (made by SGL Carbon Group), was used in the measurements. This media has uncompressed thickness of 380 μm, is treated with 5 wt%. PTFE for wet proofing, has no microporous layer, and has relatively high open porosity of 88% [27].

2.1. GDL intrusion into channel

The amount of GDL intrusion and shape change of GDL under compression must be known in order to evaluate the local parameter values of GDL. The initial GDL thickness and gasket thickness determine the deformation of GDL regardless of the compression pressure when gaskets having low compressibility are used. Hence, the measurements are conducted from the perspective of thickness, not of compression pressure.

The experimental setup is illustrated in Fig. 3. In order to control the thickness of compressed GDL, steel gages were inserted between two aluminum plates. The thickness of steel gages was varied between 150 and 350 μm. Steel gages were placed near the GDL, having an area of 1.6 cm^2, to allow precise control of the compressed GDL thickness. A channel with a width ranging from 0.6 to 2 mm was machined into the bottom aluminum plate. The parts were clamped together with four 8 mm bolts, using a torque from 0.8 to 1.5 N m, depending on the desired thickness. GDL intrusion was measured with a dial indicator (ND 221B by Heidenhain Corporation).

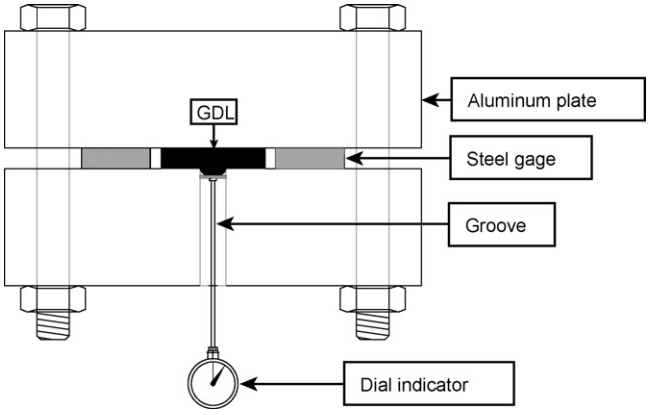

Fig. 3. Schematic illustration of GDL intrusion measurement setup.

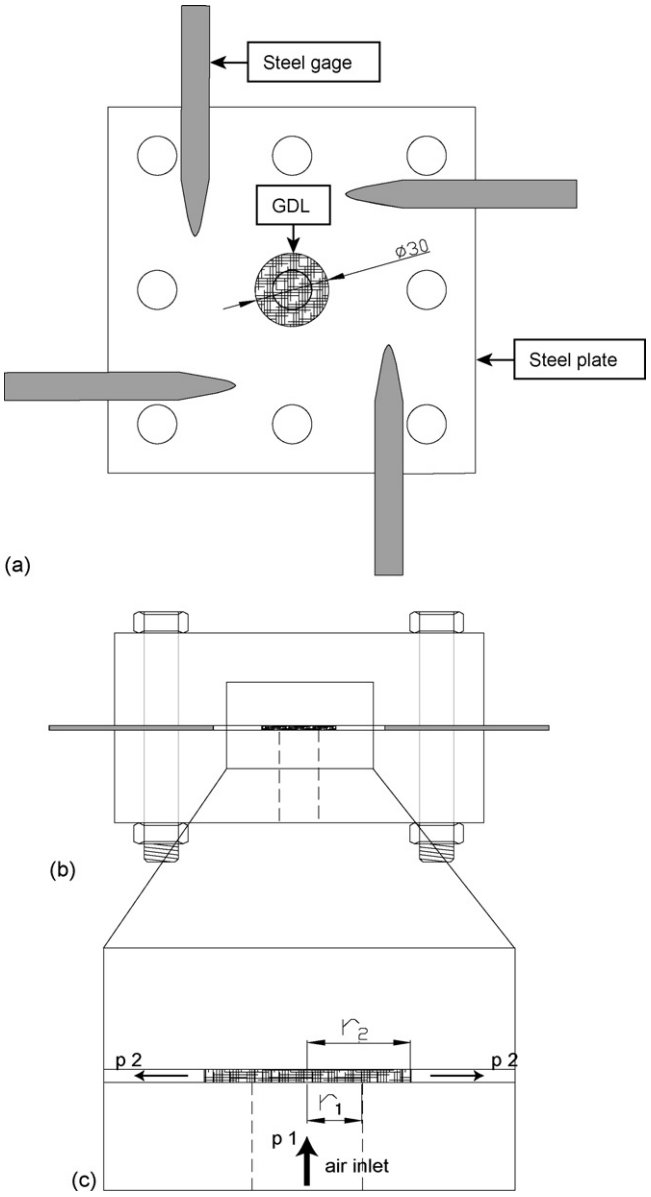

Fig. 4. Gas permeability measurement setup: (a) top view, (b) cross-section view, and (c) enlarged cross-section view.

2.2. In-plane gas permeability

The method of gas permeability measurement in this paper is fundamentally similar that used by Mikkola [28], but modified to allow the control of the thickness of GDL. The top view of the measurement device is illustrated in Fig. 4(a), and its cross-section is illustrated in Fig. 4(b) and (c). A circular GDL piece of 30 mm diameter was mounted concentrically on top of the inlet in the steel base plate. Four steel gages were situated in each corner of the base plate in order to enable the precise control of the GDL thickness. The upper base plate presses and fastens the inserted GDL and steel gages with eight bolts to ensure the assembly. The radii of air inlets, r_1, and of GDL, r_2, were 8 and 15 mm, respectively. Gas pressure at inlet r_1 was p_1 and the gas pressure p_2 at r_2 was ambient pressure, since air was discharged freely into the surroundings.

Please cite this article in press as: I. Nitta et al., J. Power Sources (2006), doi:10.1016/j.jpowsour.2006.11.018

The measurements were conducted by varying the compressed thickness of GDL from 150 to 350 μm with 50 μm steps controlled by steel gages. Dry air was used as the flowing fluid. The flow rate of air was varied in the range of 10–310 $cm^3\ min^{-1}$ controlled by a mass flow controller (Model 5850S by Brooks Instruments).

The porosity loss in GDL under compression increases the pressure drop and reduces mass transfer. The flow resistance is characterized by the gas permeability, which can be estimated by measuring pressure difference between inlet and atmosphere and by applying Darcy's law:

$$v = -\frac{k}{\eta}\nabla p \tag{1}$$

where v is the flow velocity, k the gas permeability, η the dynamic viscosity and p is the pressure. In cylindrical measurement geometry the flow can be assumed to be radially symmetric. By applying conservation of mass and ideal gas law, one can deduce the permeability from Eq. (1):

$$k = \frac{RT}{\pi V_0}\frac{\eta}{h}\frac{\dot{V}_1}{p_1^2 - p_2^2}\ln\left(\frac{r_2}{r_1}\right) = \frac{RT}{\pi V_0}\frac{\eta}{h}\frac{\dot{V}_1}{(p_m + p_2)^2 - p_2^2}\ln\left(\frac{r_2}{r_1}\right) \tag{2}$$

where $\dot{V}_1$ is the source volume flow rate, R the gas constant, T the temperature, h the cylinder height (here equivalent to compressed GDL thickness), and V_0 is the standard molar volume. The pressure difference was measured with a manometer (Type MM3K by HK Instruments Oy).

2.3. Through-plane GDL conductivity

The conventional experimental setup to evaluate the contact resistance between GDL and current collector typically consists of two graphite (or steel) current collectors, two supporting base plates, sandwiching one GDL as illustrated in Fig. 5(a), see, e.g. [10,29].

In the previous studies, various compression pressures were exerted on both sides of the base plates, which led into a change in the thickness of GDL and thus also in bulk and contact resistances. With these conditions, total resistance of the system was measured using four-point probe method. The measured total resistance $R_{z,\mathrm{meas,conv}}(z)$ with this conventional experimental setup is expressed as

$$R_{z,\mathrm{meas,conv}}(z) = 2R_{\mathrm{GR}} + R_{\mathrm{b,GDL}}(z) + 2R_{\mathrm{c,GR/GDL}}(z) \tag{3}$$

where R_{GR} and $R_{\mathrm{b,GDL}}(z)$ denote the bulk resistances of graphite current collector and GDL in through-plane direction, respectively. $R_{\mathrm{c,GR/GDL}}(z)$ is the contact resistance between graphite current collector and GDL.

The $R_{\mathrm{c,GR/GDL}}(z)$ is typically evaluated by neglecting R_{GR} and with a simple subtraction of $R_{\mathrm{b,GDL}}(z)$ which is based on the value given by manufacturer. In this conventional method, $R_{\mathrm{b,GDL}}(z)$ is considered constant and the effect of compression on the bulk conductivity of GDL is simply disregarded. In fact, the bulk conductivities of GDL strongly depend on the compression pressure as discussed in Section 3.3, and consequently this conventional method inherently contains errors in the evaluated contact resistance values.

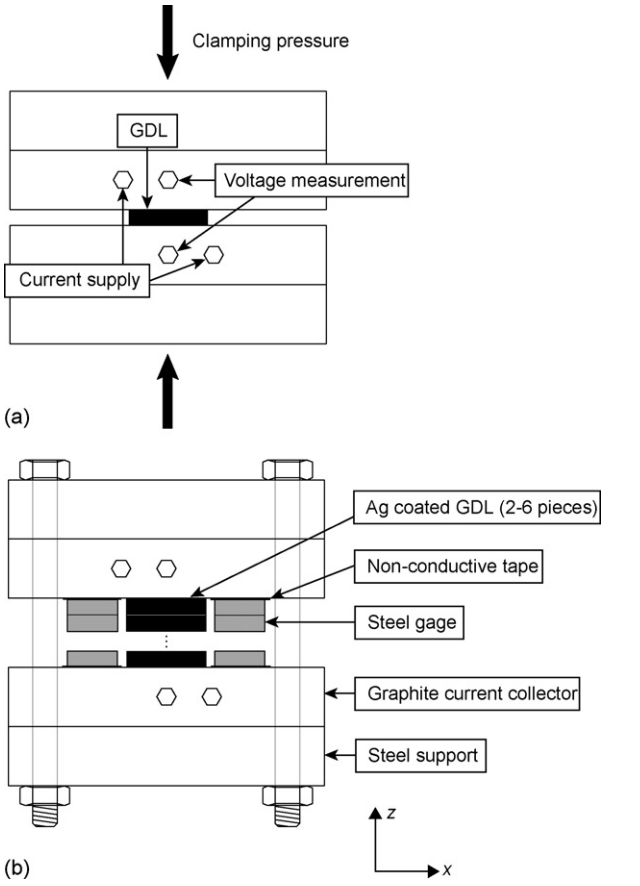

Fig. 5. Contact/bulk resistance measurement setup: (a) conventionally applied, and (b) system used in this study.

The compression pressure affects the bulk resistance of GDL and can be expressed as a function of compressed GDL thickness z:

$$R_{\mathrm{b,GDL}}(z) = \frac{z}{\sigma_{z,\mathrm{GDL}}(z)A} \tag{4}$$

where $\sigma_{z,\mathrm{GDL}}$ is the through-plane conductivity of GDL which is, in fact, a function of z, and A is the area of GDL (1.6 cm^2 in the measurements).

As shown by Nakamura et al. [29], it is intrinsically difficult to evaluate the bulk GDL resistance separately from measured total resistance since two variables ($R_{\mathrm{c,GR/GDL}}(z)$, $R_{\mathrm{b,GDL}}(z)$) are included in one Eq. (3), both of which are functions of the compressed thickness. Cunningham et al. [30] successfully isolated the bulk resistance of bipolar plate by their calibration procedures, but they could not separate the bulk and contact resistances of carbon paper.

Here, an effort is put to evaluate $R_{\mathrm{b,GDL}}(z)$ separately from the measured resistance, which allows investigation of the compression effect on GDL bulk conductivity alone. In this study, two to five pieces of GDLs were placed on top of each other as illustrated in Fig. 5(b). Non-conductive tapes were pasted on

current collectors in order to electrically isolate the end plates form each other. The thickness of each GDL was controlled by steel gages having thickness from 150 to 350 μm. For example, when three GDLs were used and each thickness of GDL was assumed to be 250 μm, the sum of thicknesses of steel gages and non-conductive tapes was set to 750 μm. This means that no matter how many GDLs were used, both $R_{c,GR/GDL}(z)$ and $R_{b,GDL}(z)$ were unchanged when the compressed thickness of GDLs was set constant. In this experimental setup, the total resistance $R_{z,meas}(n)$ which is a function of number of GDLs, n, can be expressed as

$$R_{z,\mathrm{meas}}(z,n) = 2R_{GR} + nR_{b,GDL}(z) + 2R_{c,GR/GDL}(z) + (n-1)R_{c,GDL/GDL}(z) \quad (5)$$

where $R_{c,GDL/GDL}$ is the contact resistance between two facing GDLs. If this $R_{c,GDL/GDL}$ can be eliminated from Eq. (5), it reduces into

$$R_{z,\mathrm{meas}}(z,n) = 2R_{GR} + nR_{b,GDL}(z) + 2R_{c,GR/GDL}(z) \quad (6)$$

Thus, when one plots $R_{z,meas}(n)$ as a function of number of GDLs, the slope of the graph indicates the $R_{b,GDL}(z)$. The detailed explanation about the derivation of the $R_{c,GR/GDL}(z)$ is explained in Section 2.6.

In order to eliminate $R_{c,GDL/GDL}$, highly conductive silver particles were sputtered onto GDLs. This process consisted of vacuum evaporation of coating material and deposition onto the target GDL. The deposition time was chosen so that the thickness of the silver coatings corresponds to 150 nm layer. This method was previously shown to successfully reduce the contact resistance [31,32]. According to Caillard et al. [33], the diffusion depth of deposited particles is in the range below 100 nm, which is small enough compared to the thickness of GDL in order not to affect the bulk conductivity significantly. This allowed assuming that the contact resistance between facing GDLs was negligibly small without changing the bulk properties of GDL.

All GDL surfaces that came into contact with other GDLs were silver coated, but GDL surfaces facing the graphite current collectors were left untreated. Therefore, contact resistance between the GDLs could be assumed negligible and $R_{c,GR/GDL}(z)$ could be evaluated. Resistance measurements were conducted by applying a current through the sample with 50 mA steps from 50 mA to 1 A, and simultaneously recording the voltage drop in order to calculate the total resistance.

2.4. In-plane GDL conductivity

The experimental setup used for investigation of in-plane conductivity as a function of compressed thickness of GDL is illustrated in Fig. 6. Fig. 6(a) illustrates the top view of the setup. GDL is placed on the base plate and both ends are compressed by graphite current collectors clenched with two 8 mm bolts. Steel gages were inserted between graphite current collectors and base plate, and thus the GDL thickness under the graphite current collector was always fixed to the steel gage thickness of 250 μm. The separation between two current collectors was varied in the range from 1 to 32 mm. Fig. 6(b) illustrates the cross section view of the setup. A non-conductive plastic plate was placed between the graphite current collectors. This plate allowed the accurate control of the compressed thickness of GDL underneath it and maintained the separation. The plastic plate was clamped to the base plate with two 8 mm bolts, and the thickness of GDL under plastic plate was controlled from 150 to 350 μm with steel gages.

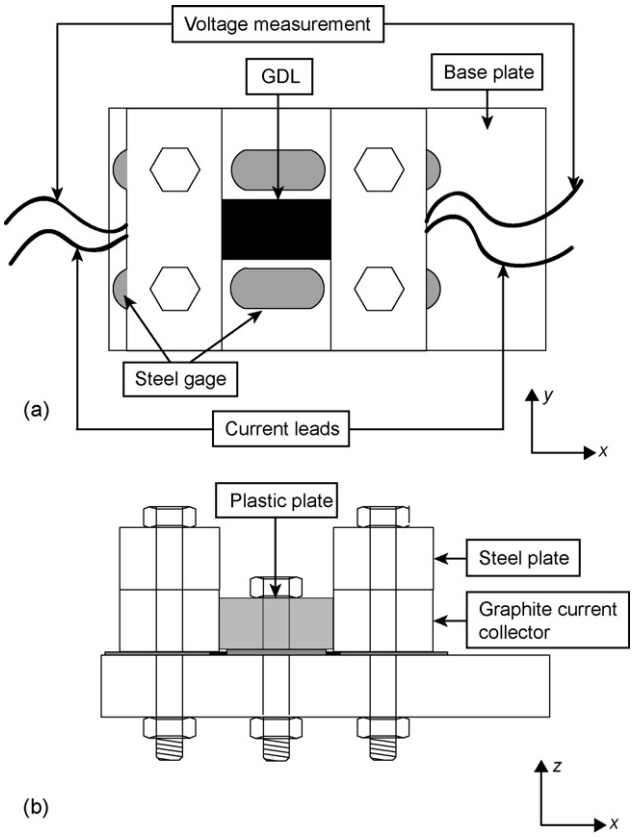

Fig. 6. In-plane conductivity measurement setup: (a) top view without plastic plate, and (b) cross section view.

A current in the range from 50 mA to 1 A with 50 mA step was applied and the voltage drop was measured to calculate the total resistance. The measured total resistance $R_{x,meas}(x,z)$ consists of the bulk resistance of graphite current collector R_{GR}, bulk resistance of GDL under the graphite current collector $R_{b,GDL}(250)$ and under the plastic plate $R_{b,GDL}(x,z)$ and the contact resistances between graphite current collector and GDL $R_{c,GR/GDL}$:

$$R_{x,\mathrm{meas}}(x,z) = 2R_{GR} + R_{b,GDL}(250) + R_{b,GDL}(x,z) + 2R_{c,GR/GDL} \quad (7)$$

In order to separate the bulk GDL resistance from the total resistance and to investigate the effect of compression, following facts and assumptions should be underlined. First, since the steel gages under graphite current collector fixed the compressed thickness of GDL to 250 μm, both $R_{c,GR/GDL}$ and $R_{b,GDL}(250)$ remained constant through the measurement series. Second, the conductivity of graphite current collector was at least one

order of magnitude larger than that of GDL, and therefore the current path within graphite current collector was assumed to concentrate to the edge of the plate and R_{GR} remained constant. And third, since the separation between the graphite plates was at least an order of magnitude larger than the thickness of compressed GDL, it was assumed that the effect of current flowing in through-plane direction from the graphite plates was negligible, allowing us to study only the changes in in-plane direction.

Based on the above facts and assumptions, $R_{b,GDL}(x,z)$ can be derived by subtracting $R_{x,meas}(x)$ from the other measured values with different separations between graphite plates. For example, with two different separation, x_1 and x_2 ($x_1 < x_2$), and with same thickness z_1, the bulk GDL resistance can be calculated from the subtraction of total resistances as

$$R_{x,meas}(x_2, z_1) - R_{x,meas}(x_1, z_1) = R_{b,GDL}(x_2 - x_1, z_1) = R_{b,GDL}(\Delta x, z_1) \quad (8)$$

Then, the in-plane conductivity $\sigma_{x,GDL}(z)$ can be calculated from the bulk resistance as

$$\sigma_{x,GDL}(z) = \frac{1}{R_{x,GDL}(\Delta x, z)} \frac{\Delta x}{zw} \quad (9)$$

where Δx, z and w are the current collector separation, compressed thickness and width (1 cm in all of the measurements) of the bulk GDL underneath the plastic plate, respectively. In order to increase the statistical accuracy, measurements were conducted using various current collector separations and the average value was used for the in-plane conductivities for each compressed thickness.

2.5. Conductivity of other components

The conductivities of graphite current collector and electrode on MEA were also evaluated by applying four-point probe method. This was done to calculate the contact resistance between GDL and electrode on MEA as explained in Section 2.4.

For determining the conductivity of graphite, a graphite block having dimensions of 8 mm × 14 mm × 90 mm was used. A current lead was connected to both ends of the block and current was applied in the range from 50 mA to 1 A. The potential drop was measured at various positions of the block with distances from 9 to 63 mm. The conductivity of graphite was solved from the subtraction of bulk resistances obtained with various lengths in similar fashion to the in-plane conductivity of GDL as described in Section 2.4.

In the evaluation of the electrode conductivity, the measurement setup was fundamentally the same as illustrated in Fig. 6, but the GDL was replaced with a piece of MEA (PRIMEA series 58 by W.L. Gore & Associates, Inc.). Since the conductivity of electrode was expected to be smaller than that of GDL, the separation between two graphite current collectors was varied from 0.5 to 10 mm and the thickness of electrode on MEA was assumed to be 10 μm. Then the same procedure as for the in-plane conductivity of GDL was applied to evaluate the conductivity of the electrode.

2.6. Contact resistance between graphite current collector and GDL

Finite element method based simulation was employed to fit the contact resistance between graphite current collector and GDL using a commercially available PDE solver program COMSOL Multiphysics 3.2a, since it was believed to be difficult to separate the contact resistance from total resistance experimentally. The conductivity of graphite was only an order of magnitude higher than that of GDL, and due to its larger thickness, the resistance of current collector also affected the results. Thus, positioning of current leads affected the profile of current going through the system, and it could not be assumed constant throughout the whole contact area of the components. Therefore, the actual measurement geometry was implemented as a 3D modeling domain. Model domain was same as the experimental setup for through-plane GDL conductivity (see Fig. 5) which was composed of two graphite current collectors and GDL sandwiched between them. The GDL thickness was changed from 150 to 350 μm in the modeling domain corresponding to the experimental study and the evaluated bulk conductivities of GDL and graphite were embedded.

The electric potential in graphite, φ_{GR}, and GDL, φ_{GDL}, were solved in the model. The governing equation for current density follows from the conservation of charge:

$$\nabla^2\varphi = \nabla(-\sigma_{z,GR}\nabla\varphi_{GR}) = \nabla(-\sigma_{z,GDL}\nabla\varphi_{GDL}) = 0 \quad (10)$$

Measured potential differences were used as boundary conditions in the model where voltage leads were attached (see Fig. 5).

Since there is a contact resistance between graphite current collector and GDL, the potential profile is discontinuous. This potential drop at the interface can be expressed with current density and the contact resistance. At the graphite current collector/GDL interface, Neumann boundary condition was applied:

$$-\bar{n}(-\sigma_{z,GR}\nabla\varphi_{GR}) = \frac{\varphi_{GR} - \varphi_{GDL}}{R_{c,GR/GDL}} \quad (11)$$

where $\bar{n}$ is the normal vector of the interface. After solving the potentials, the total current, I, passing through the system was calculated by integrating the local current density. $R_{c,GR/GDL}$ was evaluated by changing its value in the model until the total current corresponded to the measurement result. The same modeling procedure was applied to a system that consisted of various numbers of GDLs in order to find an error estimate for contact resistance.

2.7. Contact resistance between GDL and electrode on MEA

An attempt was made to evaluate the contact resistance between GDL and electrode, $R_{c,GDL/ELE}$, with fundamentally similar measurement setup and procedure as introduced in Section 2.4. The difference was that the GDL was replaced with MEA and there was GDL pieces between the graphite current collectors and MEA. The separation between two graphite current collectors was changed in the range from 0.5 to 5 mm. The

Please cite this article in press as: I. Nitta et al., J. Power Sources (2006), doi:10.1016/j.jpowsour.2006.11.018

potential profile was modeled with similar domain of in-plane experimental setup (see Fig. 6) by applying the measured total resistance and conductivities of graphite current collector, GDL and electrode, and contact resistance between GDL and graphite current collector evaluated previously. Now the only unknown parameter was the contact resistance between GDL and electrode, and its value was varied in order to fit the modeled current with the measured value similarly as in Section 2.6.

3. Results and discussion

3.1. GDL intrusion into channel under clamping pressure

The results from the measurements of GDL thickness under the channel, i.e. the sum of the measured GDL intrusion and steel gage thickness, are shown in Fig. 7. The initial thickness of GDL (380 μm) is also included in Fig. 7 for comparison. It was expected that the channel width may cause a change in GDL intrusion since the mechanical force applied onto GDL is dependent on the geometry of adjacent components (channels and ribs). However, the results indicated that the thickness of GDL under the channel is not strongly dependent on the channel width and/or the thickness of the steel gages, and it remains almost uncompressed. For example, if a 250 μm thick gasket having low compressibility is used, the GDL is compressed at maximum 10 μm under the channel regardless of the channel width.

Since the change in thickness of GDL caused by compression is mainly attributed to loss of pore volume, it naturally has an effect on mass and charge transport through the GDL. The fact that the GDL is practically not compressed under the channels leads into significant local variations in the gas permeability of the GDL, as well as electric bulk and contact resistances. This will be discussed in the following sub-sections.

3.2. In-plane gas permeability

Fig. 8 shows the calculated in-plane gas permeability of GDL as a function of compressed thickness. The gas permeability decreased non-linearly when the thickness of GDL was

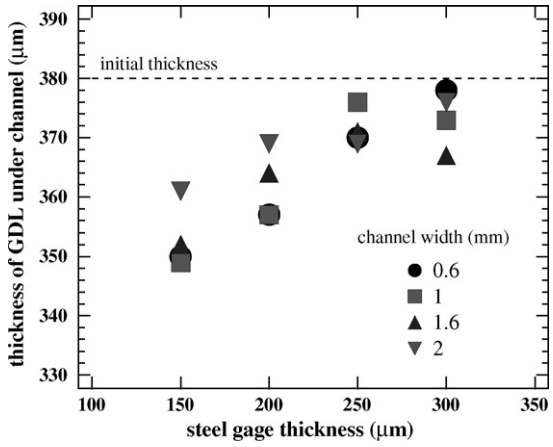

Fig. 7. Thickness of GDL under channel.

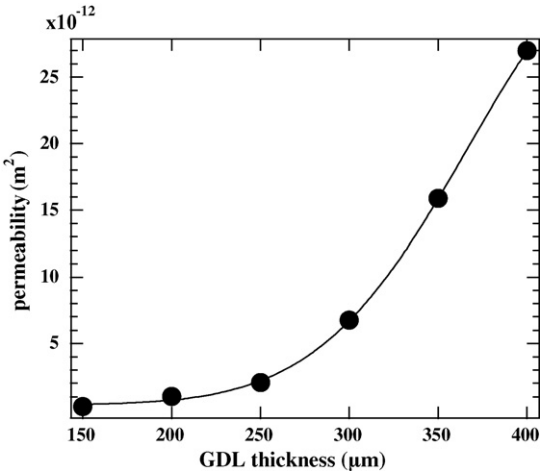

Fig. 8. In-plane gas permeability as a function of compressed thickness of GDL.

decreased by compression. The reduction in the permeability was as much as one order of magnitude when the GDL was compressed to approximately to 65% (250 μm) of the initial thickness (380 μm). The range of results is in good agreement with those published in literature for typical carbon paper type GDLs. For example, Mathias et al. [34] determined the in-plane permeability approximately to be in the range from 5×10^{-12} to 10×10^{-12} m^2 for Toray TGP-H-060 carbon paper compressed to 75% of initial thickness.

In the range where the measurements were conducted, compression of the GDL mainly leads into loss of pore volume, not compression of bulk material. Therefore, porosity can be assumed to correlate directly with compressed GDL thickness. However, most of the previous modeling studies may not directly reflect the realistic situation occurring in a fuel cell since the two above-mentioned parameters were studied separately and their combined effect was basically not considered. In fact, the compressed thickness (and thus porosity) and gas permeability of GDL are closely linked to each other as shown in Fig. 8, and it is the combined effect that determines the mass transport within the GDL.

Except for a study by Dohle et al. [6], none of experimental investigations on the effect of compressed thickness of GDL on mass transport was conducted, whereas numbers of studies focused on the initial thickness, see e.g. [35–37]. In these studies, the impact of the initial thickness on such parameters as sensitivity to water accumulation, and mass and charge transport resistance is fully addressed. However, these parameters are more closely associated with the compressed thickness of the GDL rather than the initial thickness. While the estimation of gas permeability from the porosity loss as the ratio of compressed and initial thickness is perceptive, one must note the fact that gas permeability is a non-linear function of the compressed thickness.

3.3. Through-plane and in-plane GDL conductivity

Fig. 9(a) and (b) illustrates the measured total resistance in through-plane measurement setup as a function of the number of

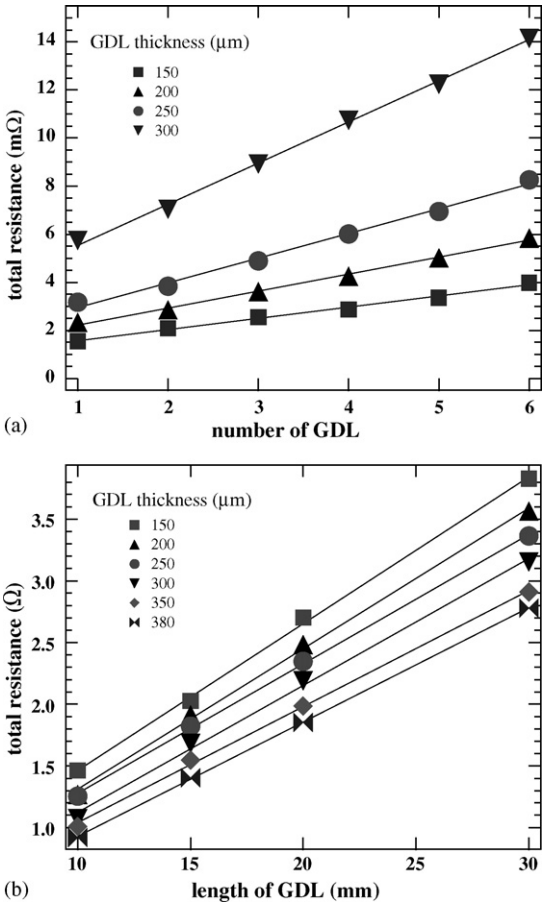

Fig. 9. Measured total resistance: (a) in through-plane direction as a function of number of GDLs, and (b) in in-plane direction as a function of length of GDL.

GDLs and the measured total resistance in in-plane measurement setup as a function of GDL length, i.e. the separation between current collectors, respectively. The results from through-plane measurements are shown for GDL thicknesses 150–300 μm for the clarity of the figure. Although the results for 350 μm behaved similarly as the other curves for different thickness, the total resistances were significantly higher and thus were not incorporated in figure. It is obvious from the results that the measured resistances are linear functions in both Fig. 9(a) and (b), and thus the in-plane and through-plane conductivity can be calculated from the linear fits (see Sections 2.3 and 2.4). The resulting values for the in-plane and through-plane conductivity of GDL as a function of compressed thickness are illustrated in Fig. 10. The achieved values are averages from several repeated measurements (5–8 measurements for each point), and the errors correspond to the standard deviations.

The conductivity in in-plane direction was three to four times higher than that in through-plane direction, which is not as large a difference as stated in the literature, see e.g. [34]. The previously reported data for GDL conductivity varies a lot even among paper type GDLs. The reported values range from 5000 to 23,000 S m^{-1} [5,7,34,38] for in-plane conductivity and from 300 to 1400 S m^{-1} [14,27,29,34] for through-plane conductivity. These variations can most probably be attributed to the physical and structural properties of different GDLs such as hydrophobic

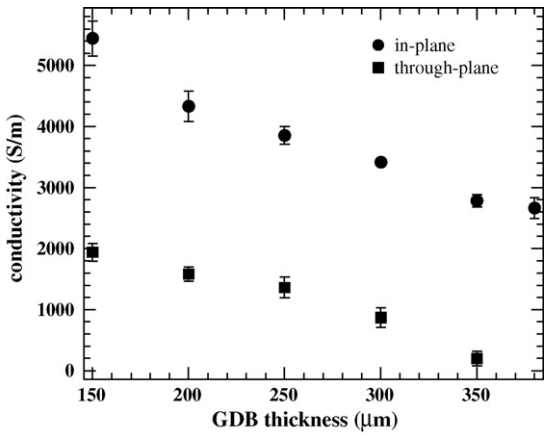

Fig. 10. In-plane and through-plane conductivities as a function of compressed thickness of GDL.

agent content, fiber diameter, density, areal density and implementation of micro porous layer. Furthermore, the significant difference in the reported conductivities may arise from the drawbacks in measurement setups and inadequate consideration of contact resistance as discussed in Section 2.3.

Both in-plane and through-plane conductivities monotonically increase as the compressed thickness of GDL was decreased. For example, when the GDL is compressed to a thickness of 250 μm, the in-plane conductivity increases 160% and through-plane conductivity over 10-fold compared to the values of uncompressed GDL. It is interesting to note that the conductivities have practically a linear dependence on the GDL compressed thickness. This is possibly because of the reduction of porosity of GDL, which leads into shorter distances between the conductive carbon fibers and also into more and better contacts between the fibers. In an assembled cell, there are significant variations in the GDL thickness between the areas under the flow channels and under the ridges. Therefore, the assumption of constant conductivity may distort modeling results significantly.

3.4. Contact resistances

The area-specific contact resistance between graphite current collector and GDL simulated by applying the conductivities presented in the previous sub-sections is given in Fig. 11. Error estimates were obtained by conducting the simulations again with considering variations in measured voltages and calculated conductivities. The contact resistance changed exponentially as a function of compressed thickness of GDL, as repeatedly reported in the literature, see e.g. [9,10,34]. Contact resistance values decreased down to two orders of magnitude from very little compression (350 μm) to high compression (150–250 μm). This result is most probably due to the fact that the actual contact area of the GDL at the interface increased with compression pressure.

There is a vast amount of literature discussing the contact resistance values, varying a lot in the range of 1–50 mΩ cm^2 with moderate compression pressure (0.5–2 MPa) [2,9,10,14,29,34,38–41]. This large variation and difference

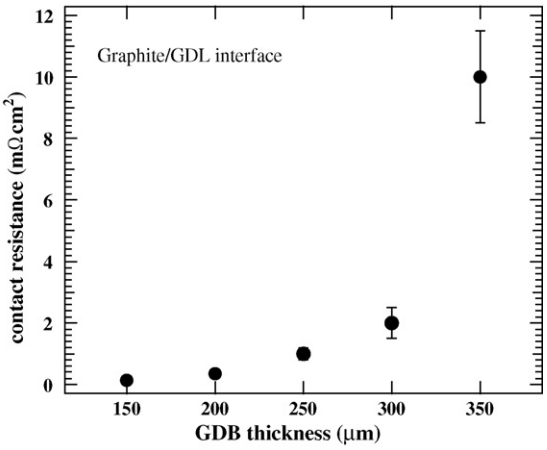

Fig. 11. Contact resistance as function of compressed thickness of GDL.

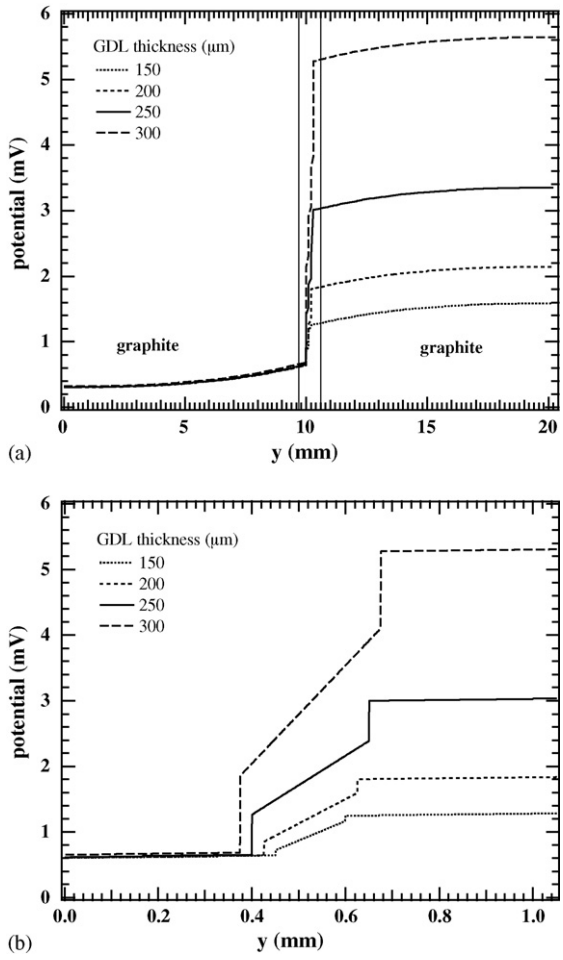

Fig. 12. Potential profiles within the model domain in longitudinal direction: (a) whole system, and (b) enlarged around the GDL.

from the values achieved in this study may be attributed to the fact that in the previous studies, the bulk resistance of the GDL and current collector was typically underestimated or simply disregarded, which in turn lead into overestimation of the contact resistance. The bulk resistance of current collector particularly has been assumed to be negligibly small because of its high conductivity in comparison to that of GDL materials, which also is often the case. For example, the conductivity of graphite used in this measurement was found to be $69700 \pm 300\,\mathrm{S\,m^{-1}}$ which was much higher than that of GDL (see Fig. 10). However, the thickness of current collector is also almost one order of magnitude larger than that of GDL because of the structure of flow field, which is typically constrained to the millimeter scale [42,43]. Thus, one cannot doubtlessly assume that the voltage drop in graphite current collector is small enough to be neglected in these measurements. Hence, it was worth investigating how significantly the bulk resistance of graphite affected the charge transport.

The electric potential profile achieved from the simulations is plotted from top to bottom at the center of x–y plane of the modeled domain (the through-plane measurement system, see Fig. 5) in longitudinal direction, as depicted in Fig. 12(a). In order to be able to distinguish the potential drop at the interfaces and in the bulk GDL, the enlarged potential profile in the region around the interface is illustrated in Fig. 12(b). According to Fig. 12(a), it is obvious that the gentle potential drop inside 1 cm thick graphite current collector at both ends ($2\Delta\varphi_{GR}$) is comparable to that caused by contact and bulk GDL resistances. It is worth noting that especially at the highest GDL compression $2\Delta\varphi_{GR}$ accounts for the dominant part of total potential drop. Hence, the resistance of current collector must be also taken into account properly when evaluating the contact resistance values in order not to distort the results. This is especially the case if the current collectors used in the measurements have lower conductivity than graphite, such as carbon compounds or polymer/graphite composites.

The potential drops caused by different factors and their relative significance are summarized in Table 1. The ratios of potential drop caused by two contact resistances and bulk GDL resistance to measured total resistance $\Delta\varphi_{meas}$, $2\Delta\phi_{R_c}/\Delta\varphi_{meas}$ and $\Delta\varphi_{GDL}/\Delta\varphi_{meas}$, respectively, are also tabulated in Table 1. Both $2\Delta\phi_{R_c}$ and $2\Delta\phi_{R_c}/\Delta\varphi_{meas}$ increased as the compressed

Table 1
Predicted voltage drops at bulk and interfaces, and percentage of them from the total measured voltage drop

Thickness (μm)	Potential drop (mV)			Ratio (%)	
	$2\Delta\phi_{R_c}$	$\Delta\varphi_{GDL}$	$2\Delta\varphi_{GR}$	$2\Delta\phi_{R_c}/\Delta\varphi_{meas}$	$\Delta\varphi_{GDL}/\Delta\varphi_{meas}$
150	0.17	0.44	0.67	8.8	23.3
200	0.42	0.74	0.67	17.1	30.4
250	1.23	1.12	0.67	33.6	30.7
300	2.35	2.24	0.67	39.4	37.6
350	6.90	6.04	0.67	51.2	44.9

Please cite this article in press as: I. Nitta et al., J. Power Sources (2006), doi:10.1016/j.jpowsour.2006.11.018

thickness of GDL was increased. However, it should be noted that $2\Delta\phi_{R_c}/\Delta\varphi_{meas}$ was unexpectedly small, whereas many sources claim that the contact resistance accounts for the major part of the total resistance, see, e.g. [9,10,29]. The results presented here highlight the fact that the contact resistances cause the major contribution to the total resistance only when the GDL is very little compressed.

These results also indicate that the bulk resistance of the GDL can make a significant contribution into the total resistance, while contact resistance was found to be smaller than previously reported. Furthermore, the effect of compression on bulk resistance cannot be neglected in the evaluation of the contact resistances. Since the bulk conductivities of GDL changed linearly with compressed thickness as shown in Fig. 10, the method used in previous studies, in which bulk conductivities are assumed constant may not yield proper values for contact resistance.

No literature data exists to verify the contact resistance between GDL and electrode on electrolyte membrane, $R_{c,GDL/ELE}$, which has typically been simply ignored in modeling. However, it can be expected that $R_{c,GDL/ELE}$ may be significantly higher than $R_{c,GR/GDL}$ since the electrode is composed also of non-electrically conductive polymer. Discussion by Ihonen [39] implies that the value may be roughly twice the value of contact resistance between GDL and graphite. $R_{c,GDL/ELE}$ is an important parameter since a high contact resistance may consequently lead into hot-spots that enhance the membrane degradation and can severely decrease the life time of fuel cells.

The $R_{c,GDL/ELE}$ obtained here by simulation for GDL thicknesses from 150 to 350 μm was in the range of 1–7 $\Omega\,cm^2$, which is far too high and thus these results are unreliable. If the contact resistance really was that high, the voltage of a unit cell would drop to zero only due to resistive losses already at the current density of approximately 500 $mA\,cm^{-2}$ with the GDL compressed to 250 μm and $R_{c,GDL/ELE}$ of 2.5 $\Omega\,cm^2$. A possible explanation for these unrealistic results is that the current profile through the electrode and GDL interface was significantly uneven. Practically all of the current concentrated to the very edge part of GDL since the graphite and GDL conductivities were significantly higher than the measured conductivity of electrode ($320 \pm 20\,S\,m^{-1}$). This may have caused numerical problems in the simulations and distorted the results. In addition, due to the low conductivity of the electrode, the separation between the graphite current collectors had to be kept very small, which led into inaccuracies in the assembly procedure of the measurement setup. However, the presented method should be applicable for the evaluation of the contact resistance between GDL and electrode, and more effort has to be put in order to achieve reliable values for it.

4. Summary and conclusions

The aim of this study was to evaluate the physical properties of GDL affected by compression in order to provide more insight into the mass and charge transport phenomena occurring in PEM fuel cells. The local properties of GDL may vary significantly due to inhomogeneous compression caused by the channel/rib structure of the flow-field plate. However, practically no previous experimental or modeling studies were found which properly consider inhomogeneous compression and its effects.

It was observed that GDL under the channel remained almost at the initial thickness regardless of the width of the channel. Slight compression of GDL under the channel was observed only at the highest compressions. The change in thickness of GDL under the rib was most probably due to the loss of porosity, and hence in an assembled fuel cell the porosity of GDL varies a lot, causing significant local variation in mass, charge, and heat transfer properties.

The in-plane gas permeability decreased non-linearly as the compressed thickness of GDL was decreased. For example, there is an order of magnitude difference in permeability between the uncompressed (380 μm) and typically compressed (250 μm) parts. The non-linear behavior may be due to changes in pore size and its distribution caused by compression.

Compression had also a notable effect on GDL bulk conductivity. Both in-plane and through-plane conductivities were practically linear functions of compressed thickness. This was most probably due to the fact that the decrease in thickness led to loss of porosity, and the distances between conductive carbon fibers were decreased and more fibers came into contact with each other.

As previously reported in the literature, contact resistance was found to vary significantly with the compression pressure. The difference in contact resistance between graphite and GDL was up to one order of magnitude between GDL compressions of 350 and 250 μm. This result may be attributed to the increase in actual contact area of GDL at the interface as the compression pressure is increased. It is worth mentioning that the magnitude of bulk resistance of both GDL and graphite current collector was comparable to the contact resistance, on the contrary to the discussions in previous studies. Thus, it is evident that the previous methods in which the bulk resistances were neglected and compression effects were disregarded may contain a considerable error in the prediction of contact resistance.

Experimental observations in this work were made using only one type of GDL media, and thus quantitative results apply only on this material. However, due to the structural similarities, the trends detected should apply also on other carbon paper and even on carbon cloth GDLs.

There are also other factors that affect the transport phenomena but are not evaluated in this study. These are the liquid water and heat transport properties. In an operating fuel cell, GDL operates in a wet environment because of the produced water. Liquid water transport may be one of the most decisive factors for the cathode performance as discussed, e.g. by Natarajan and Nguyen [44] or Lin et al. [45]. It is probable that the liquid water transport is significantly affected by the inhomogeneous compression and the consequent changes in pore size distribution. Phase change of water may be influenced by heat generated in fuel cell. Since interfaces could be one of the main heat sources in fuel cell as reported, e.g. by Noponen et al. [46], uneven distribution of electric and thermal contact resistances between GDL and electrode may create local hot spots. The hot-spots

Please cite this article in press as: I. Nitta et al., J. Power Sources (2006), doi:10.1016/j.jpowsour.2006.11.018

may even lead into accelerated degradation of membrane, and thus shorten the life time of fuel cells. The evaluation of heat and water transport parameters is left for further research.

Mass and charge transfer phenomena have a trade-off in terms of GDL compression. High compression increases GDL conductivity and decreases contact resistances, but hinders mass transfer. Thus, there may be significant differences in local cell performance. In order to gain more insight into the actual effects of the inhomogeneous compression of GDL, a modeling approach which takes into account these phenomena is needed. Such an approach is presented in the part II of this contribution [26].

Acknowledgements

The financial support of the National Technology Agency of Finland (TEKES), the Center for International Mobility (CIMO), and the Academy of Finland (project decision No. 206132) are gratefully acknowledged. In addition, the authors wish to thank Dr. Sergey Novikov from Electron Physics laboratory of Helsinki University of Technology for the silver coatings.

References

[1] W. Sun, B.A. Peppley, K. Karan, J. Power Sources 144 (2005) 42–53.
[2] P. Zhou, C.W. Wu, G.J. Ma, J. Power Sources 159 (2006) 1115–1122.
[3] W.K. Lee, C.H. Ho, J.W.V. Zee, M. Murthy, J. Power Sources 84 (1999) 45–51.
[4] J. Ge, A. Higier, H. Liu, J. Power Sources 159 (2006) 922–927.
[5] J. Ihonen, M. Mikkola, G. Lindbergh, J. Electrochem. Soc. 151 (8) (2004) A1152–A1161.
[6] H. Dohle, R. Jung, N. Kimiaie, J. Mergel, M. Müller, J. Power Sources 124 (2003) 371–384.
[7] M.V. Williams, E. Begg, L. Bonville, H.R. Kunz, J.M. Fenton, J. Electrochem. Soc. 151 (8) (2004) A1173–A1180.
[8] J.P. Feser, A.K. Prasad, S.G. Advani, J. Power Sources 162 (2006) 1226–1231.
[9] J. Ihonen, F. Jaouen, G. Lindbergh, G. Sundholm, Electrochim. Acta 46 (2001) 2899–2911.
[10] V. Mishra, F. Yang, R. Pitchumani, J. Fuel Cell Sci. Technol. 1 (2004) 2–9.
[11] H. Wang, J.A. Turner, J. Power Sources 128 (2004) 193–200.
[12] P.J.S. Vie, S. Kjelstrup, Electrochim. Acta 49 (2004) 1069–1077.
[13] M. Khandelwal, M.M. Mench, J. Power Sources 161 (2006) 1106–1115.
[14] D. Natarajan, T.V. Nguyen, J. Power Sources 135 (2004) 95–109.
[15] P.M. Wilde, M. Mandle, M. Murata, N. Berg, Fuel Cells 4 (3) (2004) 180–184.
[16] S. Escribano, J.F. Blachot, J. Etheve, A. Morin, R. Mosdale, J. Power Sources 156 (2006) 8–13.
[17] T. Matsuura, M. Kato, M. Hori, J. Power Sources 161 (2006) 74–78.
[18] H.S. Chu, C. Yeh, F. Chen, J. Power Sources 123 (2003) 1–9.
[19] T. Berning, N. Djilali, J. Power Sources 124 (2003) 440–452.
[20] D. Natarajan, T.V. Nguyen, J. Electrochem. Soc. 148 (12) (2001) A1324–A1335.
[21] G. Inoue, Y. Matsukuma, M. Minemoto, J. Power Sources 154 (2006) 8–17.
[22] J.H. Jang, W.M. Yan, C.C. Shih, J. Power Sources 156 (2006) 244–252.
[23] J.G. Pharoah, J. Power Sources 144 (2005) 77–82.
[24] H. Meng, C.Y. Wang, J. Electrochem. Soc. 151 (3) (2004) A358–A367.
[25] J.G. Pharoah, K. Karan, W. Sun, J. Power Sources 161 (2006) 214–224.
[26] T. Hottinen, O. Himanen, S. Karvonen, I. Nitta, Inhomogeneous compression of PEMFC gas diffusion layer—Part II: modeling the effect, J. Power Sources, in press.
[27] Manufacturer's Data Sheet for ®Sigracet GDL 10 BA by SGL Carbon AG.
[28] M. Mikkola, Experimental Studies on Polymer Electrolyte Membrane Fuel Cell Stacks, Master's Thesis, Helsinki University of Technology, Finland, 2001.
[29] S. Nakamura, T. Tomimura, H. Nonami, H. Saito, Proceedings of the IEEE 7th International Conference on Solid Dielectrics (2001) 101–104.
[30] N. Cunningham, M. Lefevre, G. Lebrun, J.P. Dodelet, J. Power Sources 143 (2005) 93–102.
[31] M. Yamaguchi, N. Matsuo, S. Uozumi, Japanese Patent H6-84529 (1994) (in Japanese).
[32] K. Kodama, Japanese Patent P2004-178893A (2004) (in Japanese).
[33] A. Caillarda, P. Braulta, J. Mathiasa, C. Charlesb, R.W. Boswellb, T. Sauvage, Surf. Coatings Technol. 200 (2005) 391–394.
[34] M. Mathias, J. Roth, J. Fleming, W. Lehnert, in: W. Vielstich, A. Lamm, H. Gasteiger (Eds.), Handbook of Fuel Cells, John Wiley & Sons, Ltd., New York, 2003, pp. 517–537.
[35] G. Lin, T.V. Nguyen, J. Electrochem. Soc. 152 (10) (2005) A1942–A1948.
[36] H.K. Lee, J.H. Park, D.Y. Kim, T.H. Lee, J. Power Sources 131 (2004) 200–206.
[37] L.R. Jordan, A.K. Shukla, T. Behrsing, N.R. Avery, B.C. Muddle, M. Forsyth, J. Power Sources 86 (2000) 250–254.
[38] M.M. Mench, C.Y. Wang, J. Electrochem. Soc. 150 (1) (2003) A79–A85.
[39] J. Ihonen, Development of Characterization Methods for the Components of the Polymer Electrolyte Fuel, PhD Thesis, Royal Institute of Technology (KTH), Sweden, 2003.
[40] S. Miachon, P. Aldebert, J. Power Sources 56 (1995) 31–36.
[41] H. Wang, M.A. Sweikart, J.A. Turner, J. Power Sources 115 (2003) 243–251.
[42] T. Okada, K. Ishida, M. Ishida, Japanese Patent, P2004-303558A (2004) (in Japanese).
[43] G.A. Marchetti, US Patent US 6,503,654 B2 (2003).
[44] D. Natarajan, T.V. Nguyen, J. Power Sources 115 (2003) 66–80.
[45] G. Lin, W. He, T.V. Nguyen, J. Electrochem. Soc. 151 (12) (2004) A1999–A2006.
[46] M. Noponen, E. Birgersson, J. Ihonen, M. Vynnycky, A. Lundblad, G. Lindbergh, Fuel Cells 4 (4) (2004).